University of Reading

Trends in heat stress during heat waves across Europe (1979–2023)

Article

Published Version

Creative Commons: Attribution 4.0 (CC-BY)

Open Access

Zhang, Q., Kjellsson, J., Black, E. ORCID: https://orcid.org/0000-0003-1344-6186 and Krüger, J. (2026) Trends in heat stress during heat waves across Europe (1979–2023). Geophysical Research Letters, 53 (17). e2026GL124082. ISSN 0094-8276 doi: 10.1029/2026GL124082 Available at https://centaur.reading.ac.uk/131555/

It is advisable to refer to the publisher's version if you intend to cite from the work. See Guidance on citing.

To link to this article DOI: http://dx.doi.org/10.1029/2026GL124082

Publisher: American Geophysical Union

All outputs in CentAUR are protected by Intellectual Property Rights law, including copyright law. Copyright and IPR is retained by the creators or other copyright holders. Terms and conditions for use of this material are defined in the End User Agreement.

www.reading.ac.uk/centaur

University of Reading

CentAUR

Central Archive at the University of Reading

Reading's research outputs online

Check for updates

Geophysical Research Letters

RESEARCH LETTER
10.1029/2026GL124082

Trends in Heat Stress During Heat Waves Across Europe (1979–2023)

Qi Zhang[1,2], Joakim Kjellsson[3], Emily Black[4], and Julian Krüger[5]

[1]GEOMAR Helmholtz Centre for Ocean Research Kiel, Kiel, Germany, [2]Faculty of Mathematics and Natural Sciences, Christian Albrechts University of Kiel, Kiel, Germany, [3]Swedish Meteorological and Hydrological Institute, Norrköping, Sweden, [4]University of Reading, Reading, UK, [5]Max-Planck-Institute for Meteorology, Hamburg, Germany

Key Points:

- Humidity amplifies heat stress in Northern Europe, is weak in Western and Central Europe, and partly offsets warming in the Mediterranean
- Station records show a sharp rise in alert and caution level heat stress days, extending into temperate zones
- City comparisons show greater uncertainty in humidity-driven contributions, highlighting the value of station records

Supporting Information:

Supporting Information may be found in the online version of this article.

Correspondence to:

Q. Zhang,
qzhang@geomar.de

Citation:

Zhang, Q., Kjellsson, J., Black, E., & Krüger, J. (2026). Trends in heat stress during heat waves across Europe (1979–2023). *Geophysical Research Letters*, *53*, e2026GL124082. https://doi.org/10.1029/2026GL124082

Received 11 MAY 2026
Accepted 10 AUG 2026

Author Contributions:

Conceptualization: Qi Zhang, Joakim Kjellsson
Formal analysis: Qi Zhang
Methodology: Qi Zhang
Supervision: Joakim Kjellsson
Writing – original draft: Qi Zhang
Writing – review & editing: Qi Zhang, Joakim Kjellsson, Emily Black, Julian Krüger

© 2026 The Author(s). Geophysical Research Letters published by Wiley Periodicals LLC on behalf of American Geophysical Union.
This is an open access article under the terms of the Creative Commons Attribution License, which permits use, distribution and reproduction in any medium, provided the original work is properly cited.

Abstract With heat waves becoming more frequent and intense under global warming, heat stress is a growing public health risk. We analyze heat stress trends (Simplified Wet Bulb Globe Temperature, sWBGT) during European heatwaves (1979–2023) using observations and reanalysis data. Results show widespread sWBGT increases, with distinct regional contributions from temperature and relative humidity. In Northern Europe, rising temperature and relative humidity jointly amplify heat stress. In contrast, trends in Western/Central Europe are primarily temperature-driven, whereas declining humidity partly offsets the temperature-driven increase in Mediterranean. Interaction and nonlinear residual contributions remain small. Comparisons between ERA5 and station data reveal larger differences in humidity-driven contributions, particularly in Madrid. Both data sets confirm a sharp rise in alert-level days, with Madrid experiencing a fivefold increase between the two periods. These findings clarify the spatially varying thermodynamic drivers of heat stress and highlight the expanding burden of extreme heat across temperate and southern Europe.

Plain Language Summary Global warming is making heatwaves more frequent and intense, which is a critical public health concern. To understand the true danger, we examine heat stress, which reflects the combined effects of air temperature and humidity. Humidity can make hot conditions more dangerous because it slows the evaporation of sweat, the body's main cooling mechanism. We analyzed changes in heat stress across Europe from 1979 to 2023 during heatwaves. Heat stress is rising across most of Europe, but the drivers differ by region. In Northern Europe, the risk is rising because days are becoming both hotter and more humid. In Western, Central, and Mediterranean Europe, the increase is driven mainly by rising temperatures, while declining humidity partly offsets warming in the Mediterranean. Data from major cities reveal a sharp rise in higher heat-stress conditions. For example, Madrid now experiences about five times more alert-level days than in the earlier decades. These results can support local heat safety planning and highlight the need to consider humidity as well as temperature, especially in northern regions.

1. Introduction

Heat stress has emerged as a critical public health concern, as climate change drives an unprecedented increase in the frequency and intensity of heat waves (Keellings & Moradkhani, 2020; Matthews et al., 2017; Perkins-Kirkpatrick & Lewis, 2020). For example, the 2003 European heat wave and the 2010 Russian heat wave resulted in tens of thousands of deaths (Black et al., 2004; Buzan & Huber, 2020; Russo et al., 2014). With global mean surface temperatures currently exceeding 1°C above pre-industrial levels, such conditions are becoming more common and intense (Becker et al., 2022; IPCC, 2021; King & Harrington, 2018). Heat stress has become a critical research focus with immediate societal implications (Di Napoli et al., 2023; Sherwood and Huber, 2010). Various indices have been developed to quantify heat stress, including the Heat Index (HI), Universal Thermal Climate Index (UTCI), Wet-bulb temperature (WBT), and Wet Bulb Globe Temperature (WBGT) (Budd, 2008; Casanueva et al., 2019; Di Napoli et al., 2019; Li et al., 2020; Ma et al., 2024; Steadman, 1979). The simplified Wet Bulb Globe Temperature (sWBGT) combines the effects of air temperature and atmospheric moisture and allows their respective contributions to heat stress to be quantified directly (Burgstall et al., 2019; Buzan et al., 2015). Given that Europe is warming faster than the global average (Dong & Sutton, 2025; Jacob et al., 2018), understanding regional trends in sWBGT and the respective roles of temperature and humidity is crucial for effective adaptation.

19448007, 2026, 17, Downloaded from https://agupubs.onlinelibrary.wiley.com/doi/10.1029/2026GL124082 by Emily Black - <Shibboleth>-member@reading.ac.uk , Wiley Online Library on [04/09/2026]. See the Terms and Conditions (https://onlinelibrary.wiley.com/terms-and-conditions) on Wiley Online Library for rules of use; OA articles are governed by the applicable Creative Commons License

Recent studies have documented strong increases in hot extremes and heat stress across Europe, and have shown that these changes are detectable above internal variability (Lorenz et al., 2019). Temperature extremes in western and northwestern Europe have also intensified rapidly in recent decades (Patterson, 2023; Vautard et al., 2023). Such studies have mainly focused on annual extremes, threshold exceedances, or broad scale detection of climate signals, rather than on heat stress specifically during heatwave days. The physical controls on heat stress remain regionally complex. Rising temperatures generally increase heat stress, while concurrent changes in relative humidity can strengthen or weaken this response. Previous research has shown that, on climatic time scales, relative humidity over land can decline with warming when moisture supply does not keep pace with the rising saturation vapor pressure, particularly in continental interiors with weak moisture advection (Sherwood and Fu, 2014; Byrne and O'Gorman, 2018). During hot summers, persistent blocking can further suppress moisture transport and amplify drying (Miralles et al., 2014; Pfahl & Wernli, 2012). In some regions, high humidity can coincide with high temperatures and aggravate heat stress (Founda & Santamouris, 2017). These contrasts suggest that the same temperature-defined heatwave conditions may translate into different heat stress responses across Europe.

This study examines heat stress during temperature-defined heatwave days across Europe from 1979 to 2023 using reanalysis, gridded observations, and station data. We apply an additive decomposition to quantify the temperature-driven, relative-humidity-driven, interaction, and nonlinear contributions to sWBGT changes. We assess whether these contributions differ systematically among Northern Europe, Western and Central Europe, and the Mediterranean. By comparing these patterns across multiple reanalysis and observational data sets and representative city stations, we provide a regionally resolved perspective on how dry and humid aspects of summer heat jointly influence evolving heat stress risk across Europe.

2. Data and Methods

2.1. Data

Our study focuses on European regions that have experienced several severe heatwave events, spanning from 30°N to 75°N and from 10°W to 40°E, over the period from 1979 to 2023. We focus on three European regions defined by the latest IPCC update: Northern Europe (NEU), Western and Central Europe (WCE), and the Mediterranean (MED) (Figure 1) (Iturbide et al., 2020). We calculate sWBGT using two-m temperature (T_{2m}), dew point temperature (T_{2d}), and relative humidity (RH) variables from observational and reanalysis data sets. The primary reanalysis data set is the fifth-generation European Centre for Medium-Range Weather Forecasts atmospheric reanalysis (ERA5; Hersbach et al., 2020). The ERA5 data set has an original spatial resolution of approximately 0.25° × 0.25° and hourly analysis frequency. For this study, we use instantaneous data extracted every 6 hr (00, 06, 12, 18 UTC). We also use the Japanese 55-year Reanalysis (JRA-55) data set for intercomparison with ERA5, in order to assess the robustness of our results. The JRA-55 data set has a spatial resolution of about 1.25° × 1.25° and provides instantaneous analyses every 6 hr (00, 06, 12, 18 UTC) (Kobayashi et al., 2015). High-resolution observational data (E-OBS) from the European Climate Assessment and Data set (ECA&D) is also used, which collects daily climate data fields from thousands of weather stations across Europe, into a gridded data set of 0.25° × 0.25° resolution (Cornes et al., 2018). For ERA5 we use T_{2m} and T_{2d} to calculate RH. For JRA-55, E-OBS and the city station records we use the RH variable as reported in the respective data sets. For comparative analysis across data sets, all data sets were interpolated onto a common 1° × 1° grid using bilinear interpolation. To ensure the reliability of our findings, we also include data from five meteorological stations provided by the European Climate Assessment and Data set: Oslo, Hamburg, Madrid, Vienna, and Warsaw.

2.2. Heat Wave Definition

Heatwave days are defined as periods of at least three consecutive days with maximum 2m-air temperature ($T_{2m,\ max}$) above the daily threshold for the reference period 1981–2010. The daily threshold is the 90th percentile of daily maximum temperatures, computed from a 31-day window centered on each calendar day. For a given day d, the threshold is the 90th percentile of the set of data Ad defined by

$$A_d = \bigcup_{y=1981}^{2010} \bigcup_{i=d-15}^{d+15} T_{y,i}, \tag{1}$$

where ∪ denotes the union of sets and $T_{y,i}$ is the daily $T_{2m,\ max}$ of the day i in the year y (Russo et al., 2015).

10.1029/2026GL124082

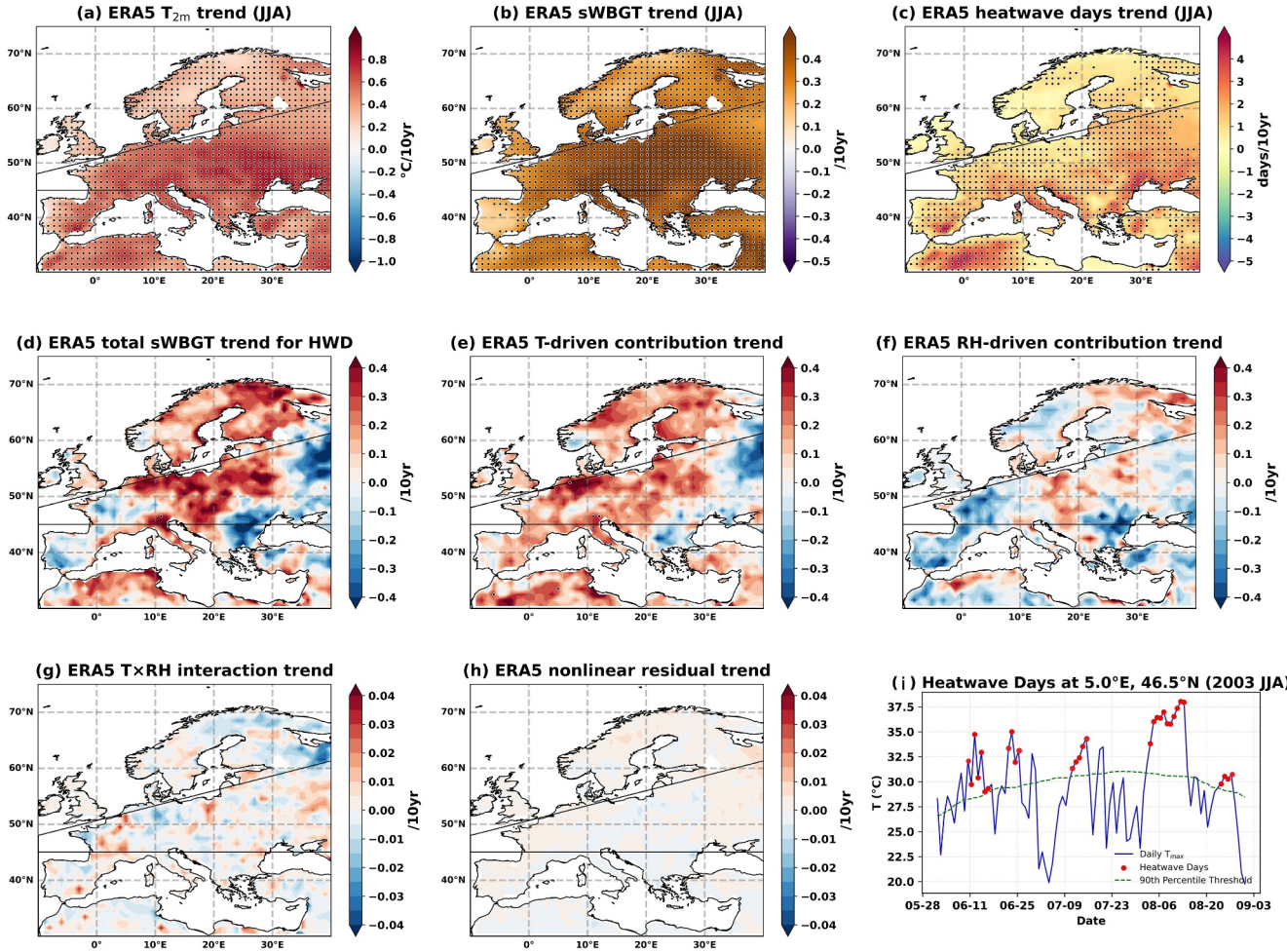

Figure 1. Trends in European summer heat stress and its drivers (1979–2023; ERA5). (a–c) Decadal trends in annual JJA mean 2m temperature (T_{2m}), annual JJA mean sWBGT, and annual number of heatwave days. (d–h) Trends during heatwave days (HWD) in total sWBGT and its temperature-driven, RH-driven, $T \times$ RH interaction, and nonlinear residual contributions, respectively. (i) Schematic of the heatwave definition using summer 2003 data at 5.0°E, 46.5°N, showing daily maximum temperatures (blue line), the 90th percentile threshold (green dashed line), and heatwave days (red dots). Stippling indicates grid cells significant after adjustment for lag-1 temporal autocorrelation and Benjamini–Hochberg false discovery rate control at $q = 0.05$.

Our definition aligns with previous studies by using a percentile threshold for daily maximum temperature and requiring a duration of at least 3 days (Katavoutas & Founda, 2019; Smid et al., 2019). Temperature-defined heatwave days are directly relevant to heat impacts, as severe heat stress can occur under extremely hot and dry conditions as well as under hot and humid conditions (Perkins-Kirkpatrick et al., 2026). Our analysis examines how RH modifies heat stress during these established heatwave conditions. Events driven primarily by unusually high humidity outside temperature-defined heatwaves may be underrepresented. We calculate heat stress and heatwave days for June–August (JJA).

2.3. Heat Stress Index Calculation

We use sWBGT as the primary index to evaluate heat stress, which incorporates both temperature and humidity effects, given by

$$\mathrm{sWBGT} = 0.56T_{2\mathrm{m}} + 0.393e(T_{2\mathrm{d}}) + 3.94, \tag{2}$$

where $T_{2\mathrm{m}}$ denotes 2m-air temperature (in °C) and e ($T_{2\mathrm{d}}$) is the vapor pressure (in hPa) at the dew point temperature (Buzan et al., 2015).

19448007, 2026, 17, Downloaded from https://agupubs.onlinelibrary.wiley.com/doi/10.1029/2026GL124082 by Emily Black - <Shibboleth-membe@reading.ac.uk , Wiley Online Library on [04/09/2026]. See the Terms and Conditions (https://onlinelibrary.wiley.com/terms-and-conditions) on Wiley Online Library for rules of use; OA articles are governed by the applicable Creative Commons License

$$e(T) = 6.1094 \exp\left(\frac{17.625T}{243.04 + T}\right), \tag{3}$$

Our calculations require vapor pressures, both calculated from Equation 3, where T is either the current air temperature (for the saturation vapor pressure, $e(T_{2m})$) or the dew point temperature (for the vapor pressure, $e(T_{2d})$). Their ratio, as shown in Equation 4, defines the RH (Alduchov & Eskridge, 1996),

$$\mathrm{RH} = \frac{e(T_{2d})}{e(T_{2m})}. \tag{4}$$

Equation 2 can therefore be expressed in terms of temperature and relative humidity as

$$\mathrm{sWBGT}(T, \mathrm{RH}) = 0.56T_{2m} + 0.393\mathrm{RHe}(T_{2m}) + 3.94. \tag{5}$$

To quantify the respective contributions of temperature and RH, we decompose sWBGT anomalies around a local reference state (T_0, RH_0), defined as the 1979–2023 mean over all valid heatwave days for each grid cell, data set, or station. The total sWBGT anomaly is

$$\Delta\mathrm{sWBGT} = \mathrm{sWBGT}(T, \mathrm{RH}) - \mathrm{sWBGT}(T_0, \mathrm{RH}_0). \tag{6}$$

Using a first-order Taylor expansion of $e(T)$ around T_0, while retaining the product of temperature and RH anomalies, the total anomaly is decomposed as

$$\Delta\mathrm{sWBGT} = \Delta s\mathrm{WBGT}_T + \Delta s\mathrm{WBGT}_{\mathrm{RH}} + \Delta s\mathrm{WBGT}_{T\times\mathrm{RH}} + \Delta s\mathrm{WBGT}_{\mathrm{res}}. \tag{7}$$

where the temperature-driven contribution is

$$\Delta s\mathrm{WBGT}_T = [0.56 + 0.393\mathrm{RH}_0 e'(T_0)](T - T_0), \tag{8}$$

the RH-driven contribution is

$$\Delta s\mathrm{WBGT}_{\mathrm{RH}} = 0.393e(T_0)(\mathrm{RH} - \mathrm{RH}_0), \tag{9}$$

and the temperature and RH interaction is

$$\Delta s\mathrm{WBGT}_{T\times\mathrm{RH}} = 0.393e'(T_0)(T - T_0)(\mathrm{RH} - \mathrm{RH}_0). \tag{10}$$

Here, $e'(T_0)$ is the temperature derivative of Equation 3 evaluated at T_0. The remaining nonlinear contribution is calculated as

$$\Delta s\mathrm{WBGT}_{\mathrm{res}} = \Delta s\mathrm{WBGT} - \Delta s\mathrm{WBGT}_T - \Delta s\mathrm{WBGT}_{\mathrm{RH}} - \Delta s\mathrm{WBGT}_{T\times\mathrm{RH}}. \tag{11}$$

This formulation is exactly additive, with the residual term retaining all remaining nonlinear contributions. Regional means of the annual values were calculated using cosine-latitude weighting:

$$\overline{X_r}(t) = \frac{\sum_{i\in V_r(t)} X_i(t)\cos\varnothing_i}{\sum_{i\in V_r(t)}\cos\varnothing_i}, \tag{12}$$

where $V_r(t)$ denotes the valid land grid cells in region r and year t, and $\varnothing_i$ is the latitude of grid cell i.

Linear trends in annual heatwave day means were estimated by ordinary least squares over 1979–2023 and are reported per decade. Trend significance was assessed using an effective sample size based on the lag-1 autocorrelation of the regression residuals, calculated only from consecutive calendar year pairs (Santer et al., 2000). For spatial maps, the resulting grid-cell p-values were additionally adjusted using the Benjamini–Hochberg false

19448007, 2026, 17, Downloaded from https://agupubs.onlinelibrary.wiley.com/doi/10.1029/2026GL124082 by Emily Black - <Shibboleth>-member@reading.ac.uk , Wiley Online Library on [04/09/2026]. See the Terms and Conditions (https://onlinelibrary.wiley.com/terms-and-conditions) on Wiley Online Library for rules of use; OA articles are governed by the applicable Creative Commons License

19448007, 2026, 17, Downloaded from https://agupubs.onlinelibrary.wiley.com/doi/10.1029/2026GL124082 by Emily Black - <Shibboleth> -member@reading.ac.uk , Wiley Online Library on [04/09/2026]. See the Terms and Conditions (https://onlinelibrary.wiley.com/terms-and-conditions) on Wiley Online Library for rules of use; OA articles are governed by the applicable Creative Commons License

discovery rate procedure at $q = 0.05$ (Benjamini & Hochberg, 1995; Wilks, 2016). Regional and city-scale trend estimates and autocorrelation-adjusted p values are summarized in Tables S1 and S2 in Supporting Information S1, respectively.

For the threshold-based analysis, sWBGT conditions were classified as Level 1 (Safe: <26.7), Level 2 (Alert: 26.7 ≤ sWBGT < 29.4), Level 3 (Caution: 29.4 ≤ sWBGT < 31.1), Level 4 (Potentially Dangerous: 31.1 ≤ sWBGT < 32.2), and Level 5 (Dangerous Conditions: ≥32.2) following Buzan et al. (2015). We adopt these ranges and labels as simple intensity classes to summarize changes in exceedance frequency, rather than as calibrated health thresholds for European populations. We note that sWBGT is a unitless variable.

3. Results

3.1. Trend Analysis of sWBGT for Heatwave Days

The summer (JJA) trends of T_{2m}, sWBGT, and heatwave days are positive across all European regions, with larger positive trends observed in WCE and MED compared to NEU (Figures 1a–1c). T_{2m} in central WCE has positive trends exceeding 0.8°C per decade. The spatial pattern of sWBGT trends (Figure 1b), calculated using Equation 2, broadly follows the T_{2m} trend pattern (Figure 1a), with predominantly positive trends across Europe. In NEU, lower baseline temperatures are associated with more moderate sWBGT increases despite ongoing warming. Central WCE shows stronger sWBGT trends, primarily attributed to higher warming rates in air temperature (Figures 1a and 1b). MED exhibits a stronger increase in the annual number of heatwave days than NEU and WCE (Figure 1c).

Using the decomposition defined in Equations 6–11, we next examine trends in total sWBGT and its individual contributions during JJA heatwave days. Positive total sWBGT trends occur across much of Scandinavia, northern Germany, the Benelux region, and central Europe, locally exceeding 0.3 per decade, whereas negative trends occur in parts of France, the Balkans, and western Russia (Figure 1d). The temperature-driven contribution broadly reproduces the spatial pattern of the total sWBGT trend, with widespread positive contributions across western, central, and northern Europe and local values also exceeding 0.3 per decade (Figure 1e). In contrast, the RH-driven contribution shows stronger regional contrasts in both sign and magnitude across Europe (Figure 1f). Negative RH-driven contributions occur across parts of western and southern Europe, including Spain, France, and the British Isles, partly offsetting the temperature-driven increase. Positive RH-driven contributions occur in parts of central and northern Europe, where they reinforce the increase in sWBGT. The $T \times \mathrm{RH}$ interaction and nonlinear residual trends are much smaller than the temperature and RH contributions across most regions (Figures 1g and 1h), indicating that the large-scale sWBGT trend patterns are mainly explained by the two first-order terms. JRA-55 and E-OBS show broadly similar temperature-driven and RH-driven patterns, while also confirming that the interaction and nonlinear residual contributions are generally small (Figures S1 and S2 in Supporting Information S1).

3.2. Contribution of T_{2m} and RH in Different Regions

To assess the regional differences in heat stress drivers, we compare annual sWBGT anomalies during heatwave days and their additive trend decomposition in observations (E-OBS) and reanalyzes (ERA5, JRA-55) (Figure 2). In NEU, all three data sets indicate positive total sWBGT trends of approximately 0.15–0.18 per decade. The temperature-driven contributions range from about 0.10 to 0.14 per decade, while the RH-driven contributions are consistently positive but smaller, at approximately 0.03–0.05 per decade (Figure 2d). Temperature therefore provides the largest contribution to the NEU trend, with increasing RH providing an additional amplification. JRA-55 and E-OBS show similar trends. The time series shows substantial interannual variability with the overall positive trend. Some peaks (e.g., in 2010) coincide with documented heatwave years in northern Europe (Rasmijn et al., 2018).

WCE shows positive total sWBGT trends of approximately 0.14–0.20 per decade across the three data sets (Figures 2b and 2e). The three annual anomaly series show broadly consistent interannual variability and long-term increases (Figure 2b). The temperature-driven contributions are of similar or slightly larger magnitude compared to NEU, ranging from about 0.15 to 0.21 per decade. In contrast, the RH-driven trends are comparatively small, ranging from approximately −0.02 to 0.04 per decade, with their sign differing among data sets. E-OBS shows a positive RH contribution, although E-OBS RH coverage is incomplete in parts of WCE. Overall, the

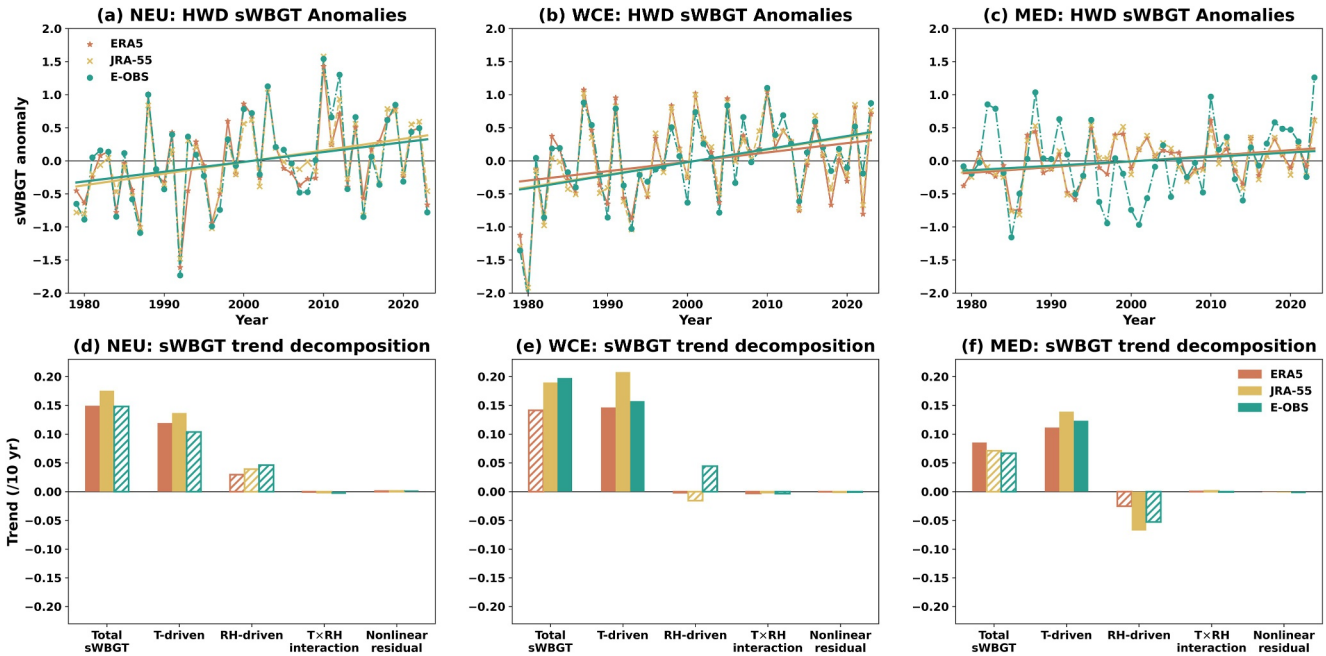

Figure 2. Regional sWBGT anomalies and trend decomposition during heatwave days, 1979–2023. (a–c) Annual sWBGT anomalies in NEU, WCE, and MED from ERA5, JRA-55, and E-OBS. (d–f) Trends in total sWBGT and its temperature-driven, RH-driven, $T \times$ RH interaction, and nonlinear residual contributions. Solid and hatched bars indicate $p < 0.05$ and $p \geq 0.05$, respectively, after lag-1 autocorrelation adjustment.

WCE increase is predominantly temperature-driven. MED presents a more complex case. As shown in Figure 2c, the annual anomaly series show larger inter-dataset differences than those in NEU and WCE, particularly for E-OBS. Total sWBGT trends remain positive under the native spatial coverage of each data set and range from approximately 0.07 to 0.09 per decade (Figure 2f). The temperature-driven contributions are positive, ranging from about 0.11 to 0.14 per decade, while the RH-driven contributions are negative, ranging from about −0.03 to −0.07 per decade. The three data sets consistently show that declining RH offsets part of the temperature-driven increase. The $T \times$ RH interaction and nonlinear residual trends remain close to zero in all three regions, generally within approximately ±0.004 per decade. The regional sWBGT trends are thus primarily explained by the first-order temperature and RH contributions. To test the influence of this spatial coverage difference, we recalculated the MED regional means for all three data sets using only grid cells with valid E-OBS coverage (Figure S3 in Supporting Information S1). The common mask analysis reveals a sign contrast between ERA5/JRA-55 and E-OBS, indicating that unequal spatial coverage alone does not explain the discrepancy.

Building on the regional analysis, we assess the agreement between ERA5 and in situ meteorological station data in five representative European cities: Oslo, Hamburg, Madrid, Vienna, and Warsaw (Figure 3). Total sWBGT trends are positive in both data sets at all five cities, with magnitudes ranging from near zero to about 0.55 per decade. The temperature-driven contribution is positive at every city, while the RH-driven contribution varies in sign and magnitude across locations and data sets. The corresponding temperature and RH time series show broad warming at all five cities, while RH trends differ among cities and between ERA5 and station records (Figure S4 in Supporting Information S1), consistent with the contrasting RH-driven contributions in Figure 3. The $T \times$ RH interaction and nonlinear residual remain small. In Oslo, ERA5 and the station record show similar total sWBGT trends of 0.20 and 0.18 per decade, respectively (Figures 3a and 3f). The temperature-driven contributions reach 0.30 and 0.25 per decade, while negative RH-driven contributions of −0.10 and −0.07 per decade partly offset the warming effect. Similar total trends are observed in Hamburg, reaching 0.24 per decade in ERA5 and 0.18 per decade in the station record (Figures 3b and 3g). The temperature-driven contribution is positive in both data sets, while the smaller RH-driven contributions differ in sign. Moving to central and eastern Europe cities, that is, Vienna and Warsaw, temperature remains the main positive contributor. Vienna shows the strongest total increase, reaching 0.45 per decade in ERA5 and 0.55 per decade in the station record (Figures 3d and 3i). RH provides an additional positive contribution in both data sets, although its magnitude differs. Warsaw shows total trends of 0.31 and 0.18 per decade in ERA5 and the station record, respectively (Figures 3e and 3j). Both data sets

19448007, 2026, 17, Downloaded from https://agupubs.onlinelibrary.wiley.com/doi/10.1029/2026GL124082 by Emily Black - <Shibboleth-member@reading.ac.uk> , Wiley Online Library on [04/09/2026]. See the Terms and Conditions (https://onlinelibrary.wiley.com/terms-and-conditions) on Wiley Online Library for rules of use; OA articles are governed by the applicable Creative Commons License

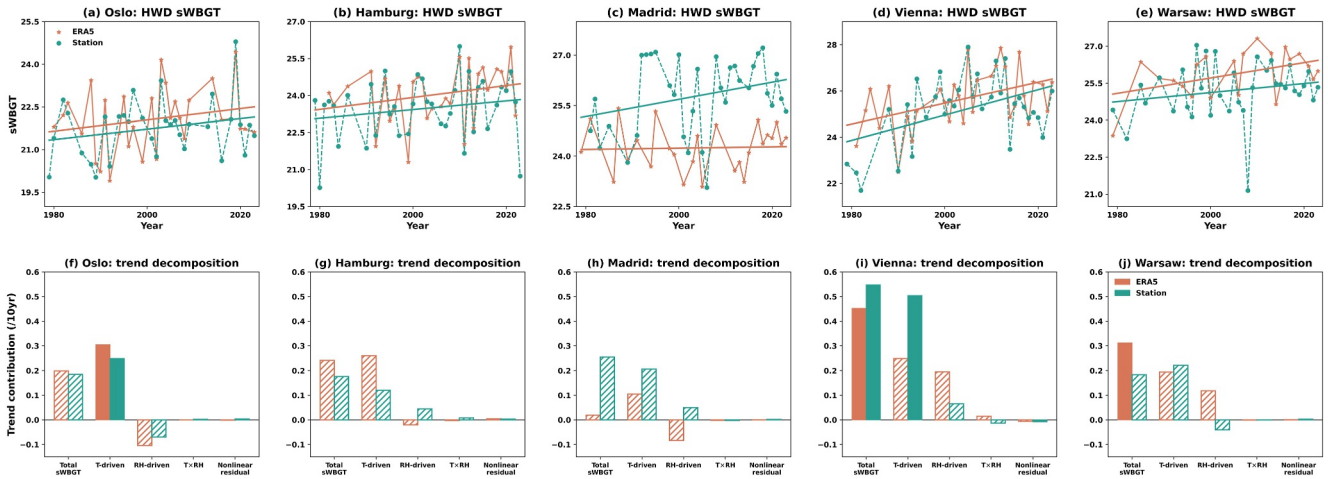

Figure 3. City-scale comparison of sWBGT during heatwave days, 1979–2023. (a–e) Annual sWBGT in Oslo, Hamburg, Madrid, Vienna, and Warsaw from ERA5 and station records. (f–j) Trends in total sWBGT and its temperature-driven, RH-driven, $T \times$ RH interaction, and nonlinear residual contributions. Solid and hatched bars indicate $p < 0.05$ and $p \geq 0.05$, respectively, after lag-1 autocorrelation adjustment.

show positive temperature-driven contributions, while the RH-driven contribution is positive in ERA5 and slightly negative in the station record. Among the five cities, Madrid displays the largest disagreement between data sets (Figures 3c and 3h). Station data show a larger positive sWBGT trend, whereas ERA5 indicates only a small positive trend. The station record combines positive temperature- and RH-driven contributions, while the ERA5 increase from temperature is largely offset by a negative RH contribution. Because sWBGT becomes more sensitive to RH at high temperatures (Figure S5 in Supporting Information S1), the contrasting RH changes produce a particularly large difference in warm Madrid. These city-scale analyses reinforce the broader result that temperature provides the main positive contribution to heat-stress trends, while the RH contribution is more spatially variable and data set dependent.

3.3. Spatial and Temporal Variations in Heat Stress Threats

To evaluate increasing heat stress levels, we classify European summer heatwave conditions using sWBGT threat levels defined in Buzan et al. (2015). Most regions, particularly the Mediterranean and Black Sea coastal zones, now experience sWBGT values within the alert (26.7–29.3) and caution (29.4–31.0) thresholds during heatwave days (Figure S6 in Supporting Information S1). Based on this finding, we analyze the total number of days of sWBGT alert and caution levels during heatwave days across Europe (Figure 4). Compared to 1979–2000, 2001–2023 shows substantial increases in both alert and caution days. The spatial distribution reveals that alert-level days are now more frequent across much of central Europe and the Mediterranean region, with the number of caution-level days also rising in southern Spain, Italy, Greece, and parts of the Mediterranean (Figures 4b and 4f). The magnitude of change is especially pronounced in the central and eastern Mediterranean, where the increase in caution days exceeds 60 days in some locations (Figure 4g). Central Europe also shows a strong rise in alert days (~80 days). In contrast, northern Europe remains largely below the alert threshold, with limited spatial expansion of heat stress levels.

Station-based comparisons in five representative cities (Oslo, Hamburg, Madrid, Vienna, Warsaw) are consistent with these regional patterns. For example, Madrid experienced an increase in alert-level days from 19 (1979–2000) to 95 (2001–2023), while Vienna rose from 17 to 70 and Warsaw from 18 to 48. Caution-level days also increased from 0 to 3 in Madrid and 2 to 5 in Warsaw. Overall, the observed rise in caution and alert-level days reflects a dual challenge of increasing intensity and geographic spread of heat stress across Europe.

4. Discussion and Conclusions

Our study quantifies the contributions of temperature and relative humidity in shaping heat stress trends during heatwave days across Europe using multiple reanalysis and observational data sets. All study regions show increasing heat stress during heatwave days, although the balance between temperature and humidity differs

19448007, 2026, 17, Downloaded from https://agupubs.onlinelibrary.wiley.com/doi/10.1029/2026GL124082 by Emily Black - <Shibboleth-member@reading.ac.uk>, Wiley Online Library on [04/09/2026]. See the Terms and Conditions (https://onlinelibrary.wiley.com/terms-and-conditions) on Wiley Online Library for rules of use; OA articles are governed by the applicable Creative Commons License

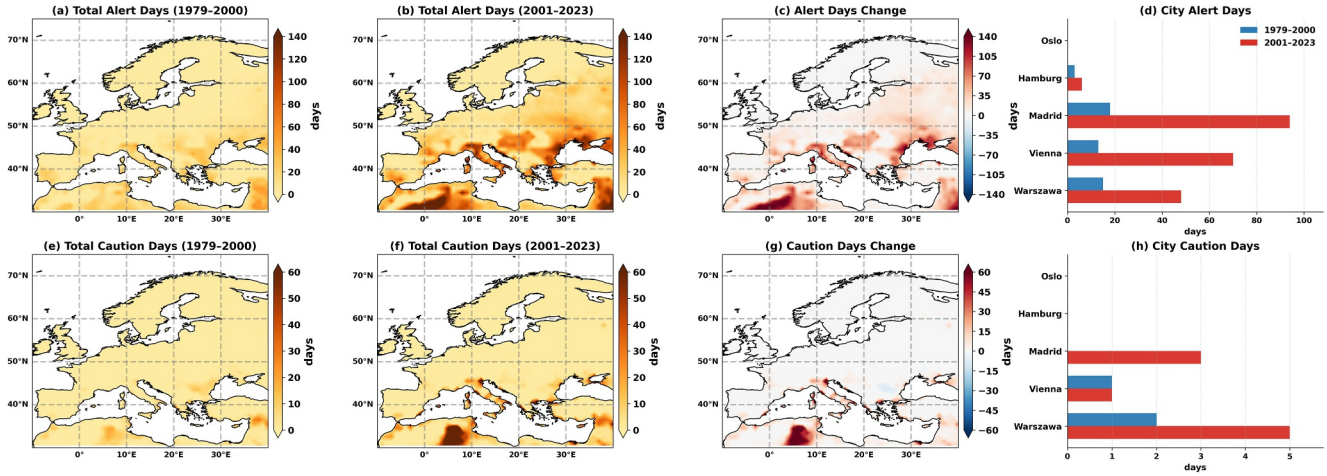

Figure 4. Spatial changes in sWBGT alert and caution level days during heatwave events between 1979–2000 and 2001–2023. (a, b) Total alert-level days during heatwave events in 1979–2000 and 2001–2023, respectively. (c) Change in alert-level days between the two periods. (d) City-scale comparison of alert-level days for Oslo, Hamburg, Madrid, Vienna, and Warsaw. (e–h) As in (a–d), but for caution-level days.

regionally. The temperature-driven contribution is positive and dominant across NEU, WCE, and MED. RH provides an additional positive contribution in NEU, has a weak and dataset-dependent regional influence in WCE, and partly offsets the temperature-driven increase in MED. The $T \times \mathrm{RH}$ interaction and nonlinear residual remain small, showing that the regional trends are primarily captured by the first-order temperature and RH contributions. City comparisons broadly support the dominant positive role of temperature and reveal stronger local variability in the RH contribution, including a negative RH contribution in Oslo despite the positive NEU regional mean and the largest inter-dataset difference in Madrid.

These results should be interpreted within a broader circulation, moisture transport, and land surface context. Changes in atmospheric circulation patterns can partly explain observed heat extreme trends (Horton et al., 2015), and recent studies further suggest that heat dome-like circulations, tropical Pacific forcing, land atmosphere coupling, and jet related changes can modulate the spatial structure and evolution of heat extremes (Cai et al., 2024; Chen et al., 2023, 2025; Lubis et al., 2024). Consistent with this broader perspective, Figure S7 in Supporting Information S1 suggests an upward shift in the regional mean moisture flux convergence anomaly during local heatwave days from the earlier to the later period, most clearly in MED, indicating a modest change in the moisture transport background associated with heatwave conditions. The widespread increase in heat stress during heatwave days is consistent with a warming background climate, while internal climate variability may modulate the regional expression of these changes on interannual to decadal timescales. Our results provide a regionally resolved diagnostic perspective on European heat stress during heatwaves and offer a basis for future attribution and process-based studies linking heat stress trends to temperature, humidity, circulation, and land surface processes.

Conflict of Interest

The authors declare no conflicts of interest relevant to this study.

Availability Statement

The ERA5 hourly single-level reanalysis data used in this study are available from the Copernicus Climate Change Service Climate Data Store (Hersbach et al., 2023). The JRA-55 reanalysis data are available from the Research Data Archive at the National Center for Atmospheric Research (Japan Meteorological Agency, 2013). The E-OBS gridded observational data are available from the Copernicus Climate Change Service Climate Data Store (Copernicus Climate Change Service, 2020). We used the 0.25° regular-grid daily temperature and relative humidity fields for 1979–2023. The city station records were obtained separately from the European Climate Assessment & Data set daily station data portal (https://www.ecad.eu/dailydata/predefinedseries.php). We used

19448007, 2026, 17, Downloaded from https://agupubs.onlinelibrary.wiley.com/doi/10.1029/2026GL124082 by Emily Black - <Shibboleth-member@reading.ac.uk>, Wiley Online Library on [04/09/2026]. See the Terms and Conditions (https://onlinelibrary.wiley.com/terms-and-conditions) on Wiley Online Library for rules of use; OA articles are governed by the applicable Creative Commons License

daily relative humidity (HU), mean temperature (TG), and maximum temperature (TX) records for Oslo, Hamburg, Madrid, Vienna, and Warsaw, corresponding to ECA&D station identifiers STAID000193, STAID000047, STAID000230, STAID000016, and STAID000209, respectively.

Acknowledgments

Qi Zhang is supported by the China Scholarship Council (CSC, Grant 202206260032). JK is supported by the OptimESM project (EU Horizon 2020, Grant 101081193). EB is supported by the EXPECT project (EU Horizon 2020, Grant 101137656, EXPECT). JKr is supported by the Hans Ertel Centre for Weather Research (HErZ) project OceanWeather (4823DWDP1B). We thank ECMWF and the Japan Meteorological Agency for providing the ERA5 and JRA-55 reanalysis data sets, and the E-OBS project for observational data. The analysis and data processing were performed on computer clusters at GEOMAR. Open Access funding enabled and organized by Projekt DEAL.

References

Alduchov, O. A., & Eskridge, R. E. (1996). Improved magnus form approximation of saturation vapor pressure. *Journal of Applied Meteorology*, *35*(4), 601–609. https://doi.org/10.1175/1520-0450(1996)035<0601:IMFAOS>2.0.CO;2

Becker, F. N., Fink, A. H., Bissolli, P., & Pinto, J. G. (2022). Towards a more comprehensive assessment of the intensity of historical European heat waves (1979–2019). *Atmospheric Science Letters*, *23*(11), e1120. https://doi.org/10.1002/asl.1120

Benjamini, Y., & Hochberg, Y. (1995). Controlling the false discovery rate: A practical and powerful approach to multiple testing. *Journal of the Royal Statistical Society: Series B*, *57*(1), 289–300. https://doi.org/10.1111/j.2517-6161.1995.tb02031.x

Black, E., Blackburn, M., Harrison, G., Hoskins, B., & Methven, J. (2004). Factors contributing to the summer 2003 European heatwave. *Weather*, *59*(8), 217–223. https://doi.org/10.1256/wea.74.04

Budd, G. M. (2008). Wet-bulb globe temperature (WBGT)—Its history and its limitations. *Journal of Science and Medicine in Sport*, *11*(1), 20–32. https://doi.org/10.1016/j.jsams.2007.07.003

Burgstall, A., Casanueva, A., Kotlarski, S., & Schwierz, C. (2019). Heat warnings in Switzerland: Reassessing the choice of the current heat stress index. *International Journal of Environmental Research and Public Health*, *16*(15), 2684. https://doi.org/10.3390/ijerph16152684

Buzan, J. R., & Huber, M. (2020). Moist heat stress on a hotter earth. *Annual Review of Earth and Planetary Sciences*, *48*(1), 623–655. https://doi.org/10.1146/annurev-earth-053018-060100

Buzan, J. R., Oleson, K., & Huber, M. (2015). Implementation and comparison of a suite of heat stress metrics within the community land model version 4.5. *Geoscientific Model Development*, *8*(2), 151–170. https://doi.org/10.5194/gmd-8-151-2015

Byrne, M. P., & O'Gorman, P. A. (2018). Trends in Continental temperature and humidity directly linked to ocean warming. *Proceedings of the National Academy of Sciences*, *115*(19), 4863–4868. https://doi.org/10.1073/pnas.1722312115

Cai, F., Liu, C., Gerten, D., Yang, S., Zhang, T., Lin, S., & Kurths, J. (2024). Pronounced spatial disparity of projected heatwave changes linked to heat domes and land-atmosphere coupling. *npj Climate and Atmospheric Science*, *7*, 1–9. https://doi.org/10.1038/s41612-024-00779-y

Casanueva, A., Kotlarski, S., Herrera, S., Fischer, A. M., Kjellstrom, T., & Schwierz, C. (2019). Climate projections of a multivariate heat stress index: The role of downscaling and bias correction. *Geoscientific Model Development*, *12*(8), 3419–3438. https://doi.org/10.5194/gmd-12-3419-2019

Chen, Z., Lu, J., Chang, C. C., Lubis, S. W., & Leung, L. R. (2023). Projected increase in summer heat-dome-like stationary waves over Northwestern North America. *npj Climate and Atmospheric Science*, *6*(1), 194. https://doi.org/10.1038/s41612-023-00511-2

Chen, Z., Lubis, S. W., Lu, J., Chang, C. C., Huang, H., Zhou, W., et al. (2025). Eastward-shifting boreal summer intraseasonal oscillation amplifies North America heatwave and wildfire risks in warming climate. *npj Climate and Atmospheric Science*, *8*, 1–14. https://doi.org/10.1038/s41612-025-01196-5

Copernicus Climate Change Service. (2020). E-OBS daily gridded meteorological data for Europe from 1950 to present derived from in-situ observations. *Copernicus Climate Change Service Climate Data Store*. [Dataset]. https://doi.org/10.24381/cds.151d3ec6

Cornes, R. C., Van Der Schrier, G., Van Den Besselaar, E. J. M., & Jones, P. D. (2018). An ensemble version of the E-OBS temperature and precipitation data sets. *Journal of Geophysical Research: Atmospheres*, *123*(17), 9391–9409. https://doi.org/10.1029/2017JD028200

Di Napoli, C., Allen, T., Méndez-Lázaro, P. A., & Pappenberger, F. (2023). Heat stress in the Caribbean: Climatology, drivers, and trends of human biometeorology indices. *International Journal of Climatology*, *43*(1), 405–425. https://doi.org/10.1002/joc.7774

Di Napoli, C., Pappenberger, F., & Cloke, H. L. (2019). Verification of heat stress thresholds for a health-based heat-wave definition. *Journal of Applied Meteorology and Climatology*, *58*(6), 1177–1194. https://doi.org/10.1175/JAMC-D-18-0246.1

Dong, B., & Sutton, R. T. (2025). Drivers and mechanisms contributing to excess warming in Europe during recent decades. *npj Climate and Atmospheric Science*, *8*(1), 41. https://doi.org/10.1038/s41612-025-00930-3

Founda, D., & Santamouris, M. (2017). Synergies between urban heat Island and heat waves in Athens (Greece), during an extremely hot summer (2012). *Scientific Reports*, *7*(1), 10973. https://doi.org/10.1038/s41598-017-11407-6

Hersbach, H., Bell, B., Berrisford, P., Biavati, G., Horányi, A., Muñoz Sabater, J., et al. (2023). ERA5 hourly data on single levels from 1940 to present. *Copernicus Climate Change Service (C3S) Climate Data Store (CDS)*. [Dataset]. https://doi.org/10.24381/cds.adbb2d47

Hersbach, H., Bell, B., Berrisford, P., Hirahara, S., Horányi, A., Muñoz-Sabater, J., et al. (2020). The ERA5 global reanalysis. *Quarterly Journal of the Royal Meteorological Society*, *146*(730), 1999–2049. https://doi.org/10.1002/qj.3803

Horton, D. E., Johnson, N. C., Singh, D., Swain, D. L., Rajaratnam, B., & Diffenbaugh, N. S. (2015). Contribution of changes in atmospheric circulation patterns to extreme temperature trends. *Nature*, *522*(7557), 465–469. https://doi.org/10.1038/nature14550

IPCC. (2021). In V. Masson-Delmotte (Ed.), et al. *Climate change 2021: The physical science basis. Contribution of working group I to the sixth assessment report of the intergovernmental panel on climate change*. Cambridge University Press. https://doi.org/10.1017/9781009157896

Iturbide, M., Gutiérrez, J. M., Alves, L. M., Bedia, J., Cerezo-Mota, R., Cimadevilla, E., et al. (2020). An update of IPCC climate reference regions for subcontinental analysis of climate model data: Definition and aggregated datasets. *Earth System Science Data*, *12*(4), 2959–2970. https://doi.org/10.5194/essd-12-2959-2020

Jacob, D., Kotova, L., Teichmann, C., Sobolowski, S. P., Vautard, R., Donnelly, C., et al. (2018). Climate impacts in Europe under +1.5°c global warming. *Earth's Future*, *6*(2), 264–285. https://doi.org/10.1002/2017EF000710

Japan Meteorological Agency. (2013). JRA-55: Japanese 55-year reanalysis, daily 3-hourly and 6-hourly data. *Research Data Archive at the National Center for Atmospheric Research, Computational and Information Systems Laboratory*. [Dataset]. https://doi.org/10.5065/D6HH6H41

Katavoutas, G., & Founda, D. (2019). Response of urban heat stress to heat waves in Athens (1960–2017). *Atmosphere*, *10*(9), 483. https://doi.org/10.3390/atmos10090483

Keellings, D., & Moradkhani, H. (2020). Spatiotemporal evolution of heat wave severity and coverage across the United States. *Geophysical Research Letters*, *47*(9), e2020GL087097. https://doi.org/10.1029/2020GL087097

King, A. D., & Harrington, L. J. (2018). The inequality of climate change from 1.5 to 2°c of global warming. *Geophysical Research Letters*, *45*(10), 5030–5033. https://doi.org/10.1029/2018GL078430

Kobayashi, S., Ota, Y., Harada, Y., Ebita, A., Moriya, M., Onoda, H., et al. (2015). The JRA-55 reanalysis: General specifications and basic characteristics. *Journal of the Meteorological Society of Japan. Series II*, *93*(1), 5–48. https://doi.org/10.2151/jmsj.2015-001

19448007, 2026, 17, Downloaded from https://agupubs.onlinelibrary.wiley.com/doi/10.1029/2026GL124082 by Emily Black - <Shibboleth-membe@reading.ac.uk>, Wiley Online Library on [04/09/2026]. See the Terms and Conditions (https://onlinelibrary.wiley.com/terms-and-conditions) on Wiley Online Library for rules of use; OA articles are governed by the applicable Creative Commons License

Li, D., Yuan, J., & Kopp, R. E. (2020). Escalating global exposure to compound heat-humidity extremes with warming. *Environmental Research Letters*, *15*(6), 064003. https://doi.org/10.1088/1748-9326/ab7d04

Lorenz, R., Stalhandske, Z., & Fischer, E. M. (2019). Detection of a climate change signal in extreme heat, heat stress, and cold in Europe from observations. *Geophysical Research Letters*, *46*(14), 8363–8374. https://doi.org/10.1029/2019GL082062

Lubis, S. W., Chen, Z., Lu, J., Hagos, S., Chang, C. C., & Leung, L. R. (2024). Enhanced Pacific northwest heat extremes and wildfire risks induced by the boreal summer intraseasonal oscillation. *npj Climate and Atmospheric Science*, *7*, 1–15. https://doi.org/10.1038/s41612-024-00766-3

Ma, Q., Chen, Y., & Ionita, M. (2024). European summer wet-bulb temperature: Spatiotemporal variations and potential drivers. *Journal of Climate*, *37*(6), 2059–2080. https://doi.org/10.1175/JCLI-D-23-0420.1

Matthews, T. K. R., Wilby, R. L., & Murphy, C. (2017). Communicating the deadly consequences of global warming for human heat stress. *Proceedings of the National Academy of Sciences*, *114*(15), 3861–3866. https://doi.org/10.1073/pnas.1617526114

Miralles, D. G., Teuling, A. J., Van Heerwaarden, C. C., & Vilà-Guerau De Arellano, J. (2014). Mega-heatwave temperatures due to combined soil desiccation and atmospheric heat accumulation. *Nature Geoscience*, *7*(5), 345–349. https://doi.org/10.1038/ngeo2141

Patterson, M. (2023). North-west Europe hottest days are warming twice as fast as mean summer days. *Geophysical Research Letters*, *50*(10), e2023GL102757. https://doi.org/10.1029/2023GL102757

Perkins-Kirkpatrick, S. E., Gregory, C. H., Vanos, J. K., Baldwin, J. W., Staudmyer, H., Guzman-Echavarria, G., & Jay, O. (2026). Deadly heat stress conditions are already occurring. *Nature Communications*, *17*(1), 2590. https://doi.org/10.1038/s41467-026-70485-1

Perkins-Kirkpatrick, S. E., & Lewis, S. C. (2020). Increasing trends in regional heatwaves. *Nature Communications*, *11*(1), 3357. https://doi.org/10.1038/s41467-020-16970-7

Pfahl, S., & Wernli, H. (2012). Quantifying the relevance of atmospheric blocking for co-located temperature extremes in the northern hemisphere on (sub-)daily time scales. *Geophysical Research Letters*, *39*(12), 2012GL052261. https://doi.org/10.1029/2012GL052261

Rasmijn, L. M., Van Der Schrier, G., Bintanja, R., Barkmeijer, J., Sterl, A., & Hazeleger, W. (2018). Future equivalent of 2010 Russian heatwave intensified by weakening soil moisture constraints. *Nature Climate Change*, *8*(5), 381–385. https://doi.org/10.1038/s41558-018-0114-0

Russo, S., Dosio, A., Graversen, R. G., Sillmann, J., Carrao, H., Dunbar, M. B., et al. (2014). Magnitude of extreme heat waves in present climate and their projection in a warming world. *Journal of Geophysical Research: Atmospheres*, *119*(22). https://doi.org/10.1002/2014JD022098

Russo, S., Sillmann, J., & Fischer, E. M. (2015). Top ten European heatwaves since 1950 and their occurrence in the coming decades. *Environmental Research Letters*, *10*(12), 124003. https://doi.org/10.1088/1748-9326/10/12/124003

Santer, B. D., Wigley, T. M. L., Boyle, J. S., Gaffen, D. J., Hnilo, J. J., Nychka, D., et al. (2000). Statistical significance of trends and trend differences in layer-average atmospheric temperature time series. *Journal of Geophysical Research*, *105*(D6), 7337–7356. https://doi.org/10.1029/1999JD901105

Sherwood, S., & Fu, Q. (2014). A drier future? *Science*, *343*(6172), 737–739. https://doi.org/10.1126/science.1247620

Sherwood, S. C., & Huber, M. (2010). An adaptability limit to climate change due to heat stress. *Proceedings of the National Academy of Sciences*, *107*(21), 9552–9555. https://doi.org/10.1073/pnas.0913352107

Smid, M., Russo, S., Costa, A. C., Granell, C., & Pebesma, E. (2019). Ranking European capitals by exposure to heat waves and cold waves. *Urban Climate*, *27*, 388–402. https://doi.org/10.1016/j.uclim.2018.12.010

Steadman, R. G. (1979). The assessment of sultriness. Part I: A temperature-humidity index based on human physiology and clothing science. *Journal of Applied Meteorology and Climatology*, *18*(7), 861–873. https://doi.org/10.1175/1520-0450(1979)018<0861:TAOSPI>2.0.CO;2

Vautard, R., Cattiaux, J., Happé, T., Singh, J., Bonnet, R., Cassou, C., et al. (2023). Heat extremes in Western Europe increasing faster than simulated due to atmospheric circulation trends. *Nature Communications*, *14*(1), 6803. https://doi.org/10.1038/s41467-023-42143-3

Wilks, D. S. (2016). "The stippling shows statistically significant grid points": How research results are routinely overstated and overinterpreted, and what to do about it. *Bulletin of the American Meteorological Society*, *97*(12), 2263–2273. https://doi.org/10.1175/BAMS-D-15-00267.1

19448007, 2026, 17, Downloaded from https://agupubs.onlinelibrary.wiley.com/doi/10.1029/2026GL124082 by Emily Black - <Shibboleth>-member@reading.ac.uk , Wiley Online Library on [04/09/2026]. See the Terms and Conditions (https://onlinelibrary.wiley.com/terms-and-conditions) on Wiley Online Library for rules of use; OA articles are governed by the applicable Creative Commons License